

## STRAIN HARDENING BEHAVIOR OF DUAL PHASE, NON-GRAIN ORIENTED ELECTRICAL AND AISI 304 STEELS\*

Guilherme Corrêa Soares<sup>1</sup>  
Berenice Mendonça Gonzalez<sup>2</sup>  
Leandro de Arruda Santos<sup>3</sup>

### Abstract

Deeper understanding about the strain hardening behavior of steels has become necessary due to its importance in industrial processes such as mechanical cold forming, rolling and drawing. In this work, the strain hardening behavior of AISI 304, non-grain oriented electrical (NGO) and dual phase steels was investigated. Tensile tests were performed and the strain hardening behavior of each steel was studied by the Hollomon's equation. X-ray diffraction measurements and hardness tests were also carried out in order to characterize the specimens. Different work hardening stages were observed in each steel during the deformation process. The results obtained are discussed in terms of the relationship among the instantaneous strain hardening coefficient, hardness and eventual phase transformations. The instantaneous strain hardening coefficient of dual phase and NGO increases after the yield point, rapidly reaching its maximum and then steadily decreases until tensile strength is reached. In AISI 304's case, the strain hardening coefficient keeps raising to high values in response to a large strain and then rapidly decreases before reaching the tensile strength. In comparison to the other steels, AISI 304 shows higher instantaneous strain hardening coefficient value, which persists even in large strains. This is a consequence of its strain hardening mechanism based on stress-induced martensite transformation.

**Keywords:** Strain hardening; Mechanical properties; Instantaneous  $n$  value; Stress-induced martensite.

<sup>1</sup> Undergraduate student, Metallurgical Engineering, Universidade Federal de Minas Gerais (UFMG), Belo Horizonte, MG, Brasil.

<sup>2</sup> Physicist, Ph.D., Professor, Department of Metallurgical and Materials Engineering, Universidade Federal de Minas Gerais (UFMG), Belo Horizonte, MG, Brasil.

<sup>3</sup> Engineer, Ph.D., Professor, Department of Metallurgical and Materials Engineering, Universidade Federal de Minas Gerais (UFMG), Belo Horizonte, MG, Brasil.

## 1 INTRODUCTION

Material researchers have been lately focused on structural materials for the automotive and aerospace industry, vital areas for transportation systems, mechanical and architectural structures. Therefore, the lightweighting of components used in such areas is essential and it is seen as the most efficient way of improving fuel usage and reduce carbon emissions [1,2]. There has been effort to develop materials with an optimal combination among mechanical properties, costs and productivity [3].

Strain hardening is an essential industrial process, which is mainly used to harden alloys that are not responsive to heat treatment [4]. Thus, better understanding of strain hardening behavior is essential in enhancing the parameters for metal forming, since it is intimately associated to cold workability [1].

One important parameter to measure the ability of a material to be strain hardened is the strain hardening coefficient,  $n$ . As shown in other studies [1,2], the strain hardening coefficient is not constant and changes during plastic deformation. Therefore, a true strain-dependent coefficient is more adequate to describe the correct strain hardening behavior of a material [5].

Based on the Hollomon's equation, Dieter [4] defined the differential equation (1) for the strain hardening coefficient as:

$$n = \frac{d(\ln \sigma)}{d(\ln \varepsilon)} \quad (1)$$

In equation (1)  $n$  is the instantaneous strain hardening coefficient,  $\sigma$  represents true stress and  $\varepsilon$  true strain. This method was considered to represent very nearly the actual behavior of steel under uniaxial tension, being considered to be used for accurate prediction during forming operations [6].

The purpose of the present work is to investigate the instantaneous strain hardening coefficient of the AISI 304, non-grain oriented electrical and dual phase steels during uniaxial tensile tests at room temperature. These results were analyzed based on the Hollomon's equation. The microstructural and hardening evolution during deformation was also investigated by X-ray diffraction (XRD) and hardness tests.

## 2 MATERIAL AND METHODS

Three different metal sheet specimens were used in this work: an AISI 304 stainless steel, a non-grain oriented electrical steel and a dual phase steel. The chemical composition of steels used in this work is given in Table 1.

**Table 1.** Chemical composition of the steel investigated ( in wt%)

Steel	C	Mn	Si	P	S	Cr	Ni	Al
AISI 304	0.0427	0.0039	0.3597	0.0247	0.0018	18.1023	8.0261	0.0024
NGO	0.0039	1.1773	2.1278	0.0131	0.0003	-	-	0.0024
DP	0.10	1.8	0.51	0.018	0.007	-	-	0.035

Specimens for the tensile test were cut into Sheet-Type Specimen according to ASTM A370 standards [7]. Both dual phase and non-grain oriented electrical steels were cut into several subsize specimens measuring 100 x 10 x 1.2 mm and 100 x 10 x 0.5 mm respectively. The AISI 304 test specimens were cut into standard specimen size, measuring 200 x 20 x 1 mm.

The gauge length and width of test specimens were measured with a profile projector PJ311 (Mitutoyo, Chicago, IL, USA) and used in each tensile test afterwards.

Work hardening behavior and mechanical properties were investigated through uniaxial tensile tests, which were conducted at room temperature and at a constant strain rate of  $1 \times 10^{-3} \text{ s}^{-1}$  using an Instron 5582 machine (Instron, Canton, MA, USA). Both dual phase and non-oriented grain electrical steels were deformed until rupture, while the AISI 304 was deformed in 5 different true strain values, being those 0.1; 0.2; 0.3; 0.4 and until rupture. This was done so the stress-induced martensitic transformation that occurs during deformation could be observed in X-ray diffraction. Hardness analysis was performed on dual phase and AISI 304 steels, using a Zwick & Co.KG. machine Model Z302 (Ulm, BW, Germany).

To determine the constituent phases on each steel, X-ray diffraction (XRD) patterns were measured using a Philips PW 1710 ( Philips Instrument, Eindhoven, The Netherlands) with a Bragg-Brentano geometry and using  $\text{Cu K}\alpha$  radiation ( $\lambda=0.15418\text{nm}$ ). These were obtained at room temperature, in a range of  $20^\circ$  to  $90^\circ$  and  $0.02^\circ/\text{s}$  step.

### 3 RESULTS AND DISCUSSION

The results of this work pointed out to the fact that the strain hardening coefficient is not constant and it is regularly varying with the increasing of the strain. Results indicate that strain hardening occurs in distinct stages, differing according to chemical composition, and microstructure. These conclusions are in agreement with results found in older publications [2-9].

#### 3.1 Dual Phase Steel

Results from tensile testing for the dual phase steel indicate a 345 MPa yield strength, 664 MPa tensile strength and a 33% total elongation. Fig. 1a shows its engineering stress-strain curve and its flow curve is shown in Fig. 1b. The strain hardening rate ( $d\sigma/d\varepsilon$ ) is derivative from the flow curve and it is plotted in Fig. 1c as function of the true strain. It is clear that the strain hardening rate decreases with the increasing of the true strain values. Fig. 1d shows the instantaneous strain hardening coefficient as a function of the true strain and indicates that the strain hardening behavior can be divided into two different regions during uniform deformation. Region 1 is between yield point and  $\varepsilon = 0.031$ , in which the strain hardening coefficient increases rapidly to its maximum. Region 2 is found after  $\varepsilon = 0.031$  until tensile strength and shows a steadily decreasing strain hardening coefficient.

Fig 2 shows the XRD patterns for the Dual Phase steel before and after deformation. Two main differences can be observed between the patterns: 1) absence of austenite after deformation; 2) enlargement of the peaks. The absence of austenite is explained by phase transformation induced by stress, resulting in martensite. The enlargement of peaks is always expected in deformed structures because of the introduction of defects in that. Hardness as a function of the true strain is shown in Fig 3. Even though hardness doesn't increase in the same rate as tensile strength, it increases with higher strains, which corroborates with strain hardening.

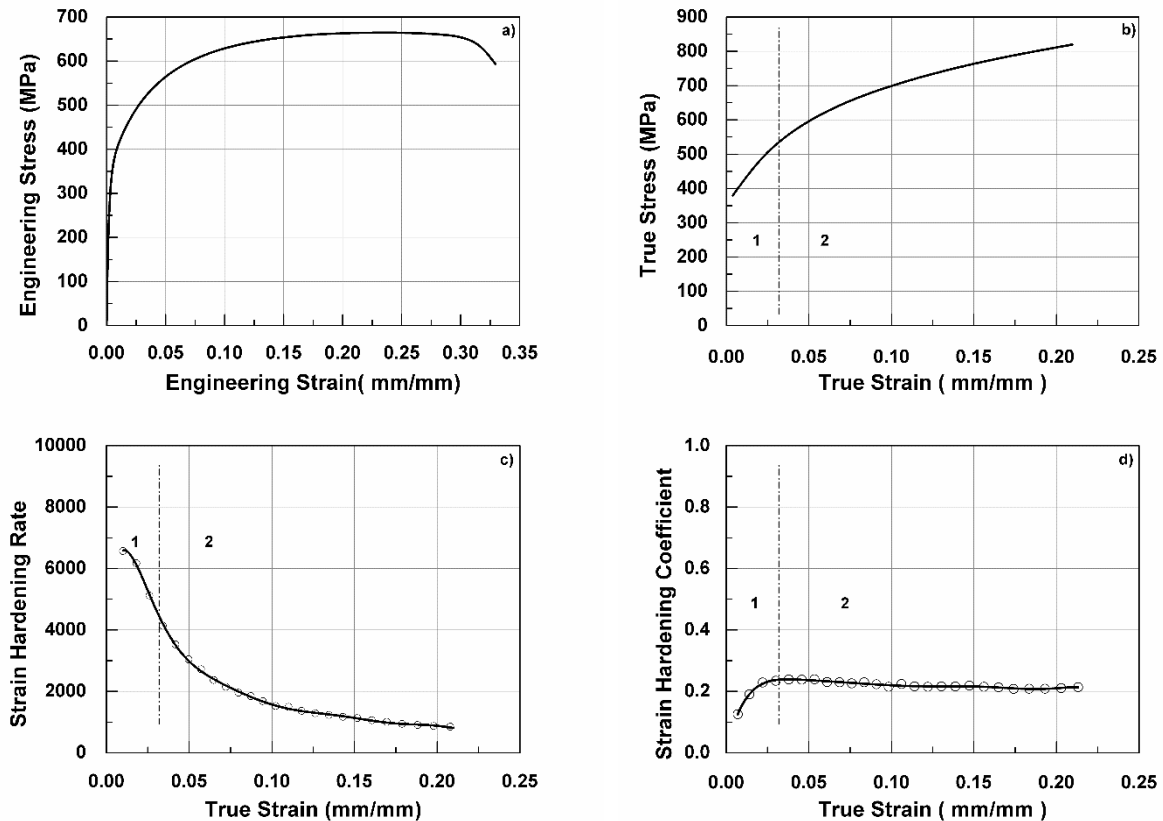


**Figure 1.** Engineering stress-strain curve (a), flow curve (b), strain hardening rate as a function of true strain (c) and instantaneous strain hardening coefficient as a function of the true strain (d) of a dual phase steel.

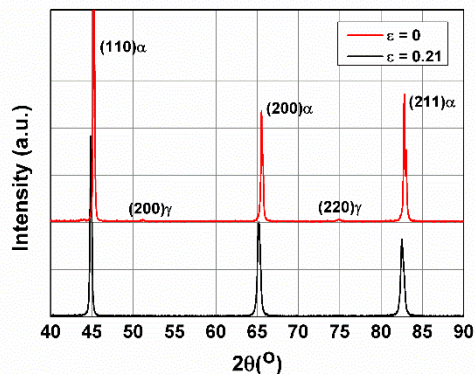


**Figure 2.** X-ray diffraction pattern of dual phase steel before and after deformation.

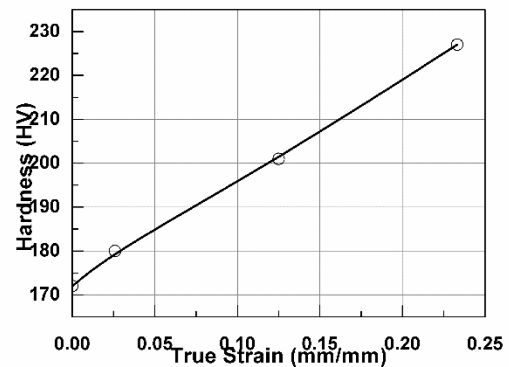
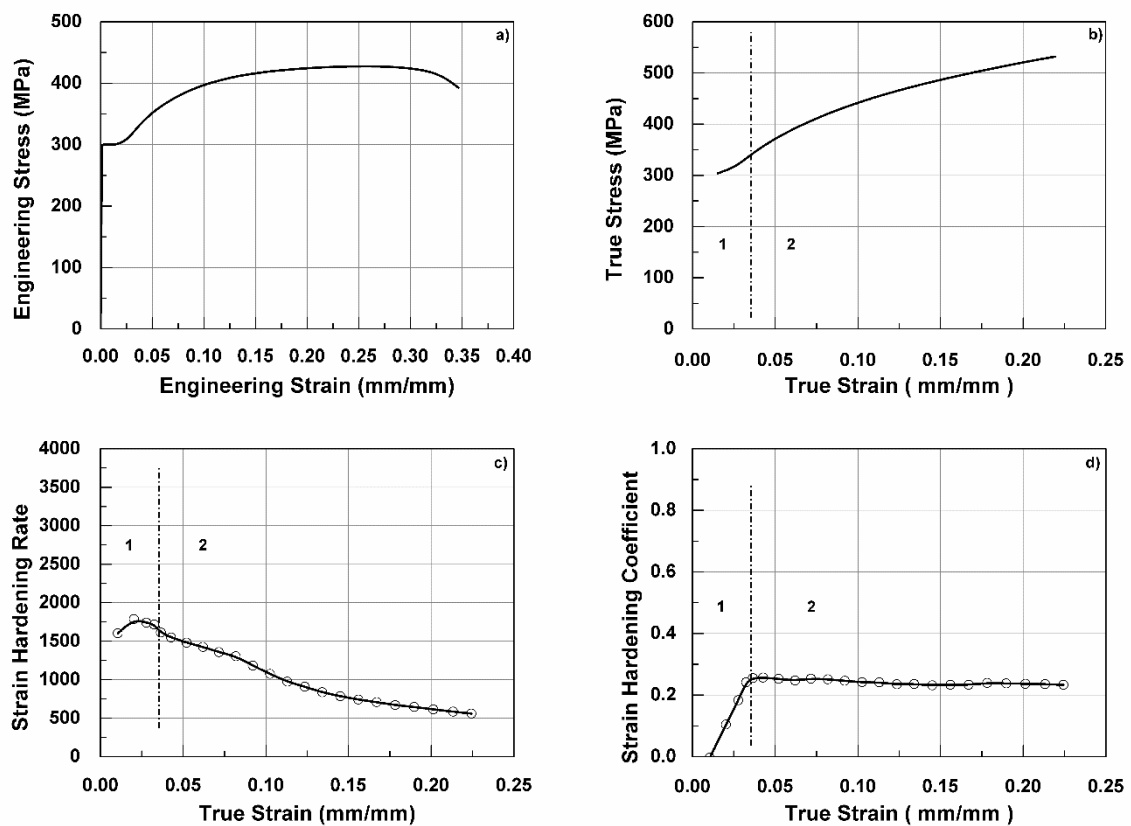


**Figure 3.** Hardness of dual phase steel as a function of the true strain.

### 3.2 Non-grain Oriented Electrical Steel

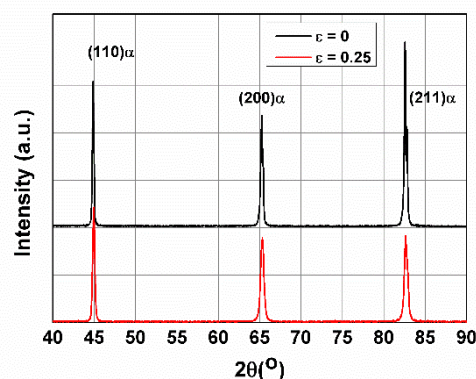
Results from tensile testing for the non-grain oriented electrical steel indicate a 303 MPa yield strength, 430 MPa tensile strength and a 34% total elongation. Fig. 4a shows its engineering stress-strain curve. It is notable that this non-grain oriented electrical steel exhibits discontinuous yield. The flow curve is shown in Fig. 4b. The strain hardening rate ( $d\sigma/d\varepsilon$ ) is shown in Fig. 4c, as a function of the true strain. As in the dual phase steel, the strain hardening rate also decreases with the increasing in

the true strain values, but there is a small increase during lower strain. Fig. 4d shows the instantaneous strain hardening coefficient as function of the true strain, and it indicates that the strain hardening behavior can be divided into two different regions. Region 1 is between yield point and  $\varepsilon = 0.035$ , in which the strain hardening coefficient increases rapidly to its maximum. Region 2 is extended from  $\varepsilon = 0.035$  until tensile strength and shows a slowly steadily decreasing strain hardening coefficient. Both dual phase and non-grain oriented electrical steel have a similar strain hardening behavior.



**Figure 4.** Engineering stress-strain curve (a), flow curve (b), strain hardening rate as a function of true strain (c) and instantaneous strain hardening coefficient as a function of true strain (d) of a non-grain oriented electrical steel.

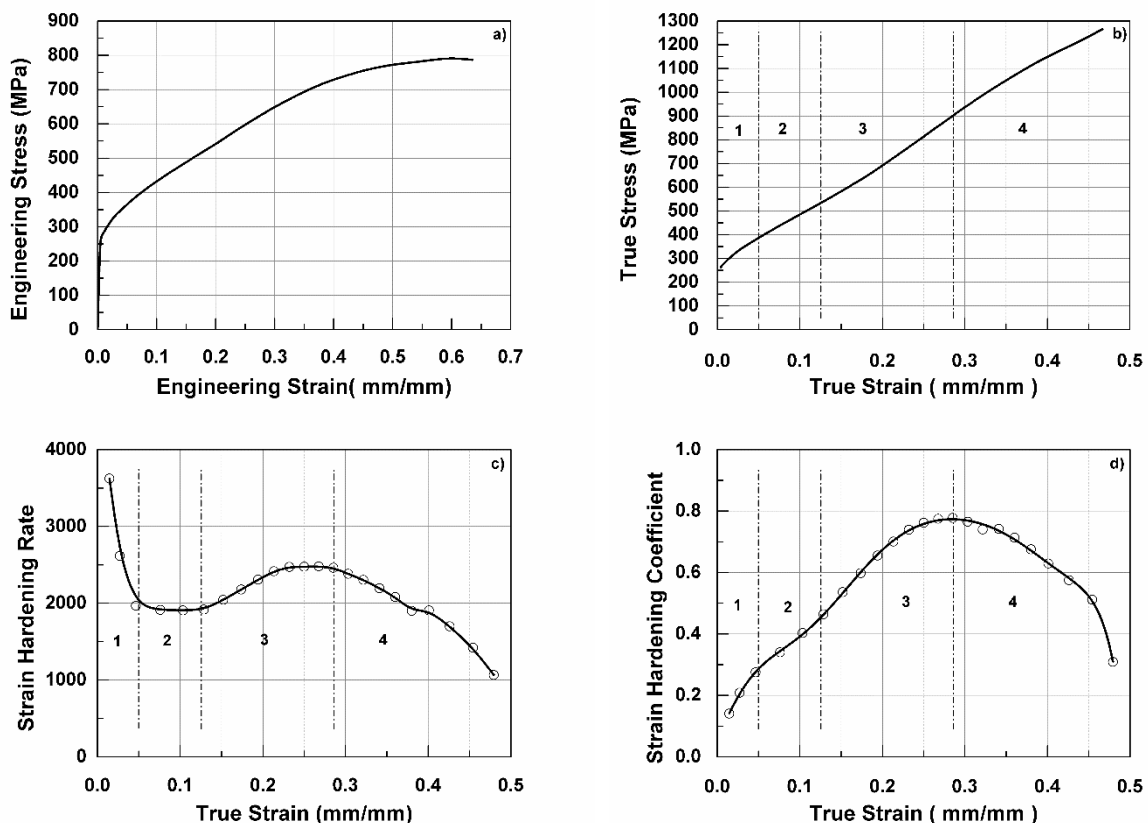
Fig. 5 shows the XRD patterns before and after deformation. The intensity of peaks is reduced and the broadening of the peaks is observed after plastic deformation due to the increased number of microstructure defects.



**Figure 5.** X-ray diffraction pattern of non-grain oriented steel before and after deformation.

### 3.3 Stainless AISI 304 Steel

Results from tensile testing for the stainless AISI 304 steel indicate a 272 MPa yield strength, 800 MPa tensile strength and a 63% total elongation. The stainless AISI 304 has certainly a higher tensile strength and longer total elongation. Therefore, it has greater strain hardening capabilities than the other two analysed steels. Fig. 6a shows its engineering stress-strain curve and flow curve is shown in Fig. 6b. Strain hardening rate ( $d\sigma/d\varepsilon$ ) and instantaneous strain hardening coefficient are respectively plotted in Fig. 6c and Fig. 6d. Strain hardening rate and strain hardening coefficient indicated that the strain hardening behavior can be divided into four different regions. Region 1 is between yield point and  $\varepsilon = 0.05$ , in which the strain hardening coefficient increases but the strain hardening rate sharply falls. Region 2 is extended between  $\varepsilon = 0.05$  until  $\varepsilon = 0.09$ , showing still increasing strain hardening coefficient and a constant strain hardening rate. Region 3 is between  $\varepsilon = 0.09$  and  $\varepsilon = 0.285$ , in which both strain hardening rate and strain hardening coefficient raise, having the strain hardening coefficient reached its maximum. Region 4 is the last one and it is found after  $\varepsilon = 0.028$ , both strain hardening rate and coefficient fall with the true strain increasing.



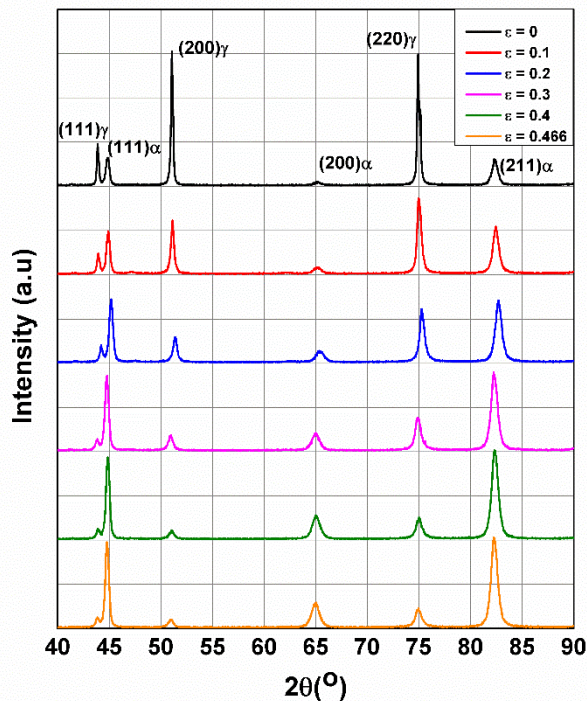
**Figure 6.** Engineering stress-strain curve (a), flow curve (b), strain hardening rate as a function of true strain (c) and instantaneous strain hardening coefficient as a function of true strain (d) of a stainless AISI 304 steel.

Fig. 7 shows the XRD pattern of the AISI 304 stainless steel for six different true strain values ( $\varepsilon = 0$ ;  $\varepsilon = 0.1$ ;  $\varepsilon = 0.2$ ;  $\varepsilon = 0.3$ ;  $\varepsilon = 0.4$ ;  $\varepsilon = 0.466$ ). Initially, austenite is the major phase revealed by XRD analysis, some small amount of martensite is also revealed. With the advance of the deformation, austenite goes through a stress-induced martensitic transformation, which is an important strain hardening

mechanism in these steels. It is noticeable that the martensitic transformation reaches its end between  $\varepsilon = 0.3$  and  $\varepsilon = 0.4$ . After deformation, XRD analysis reveals martensite as the major phase and detects some austenite. Fig. 8 shows that AISI 304 has a 180% hardness increase after plastic deformation, which also points out to its great strain hardening capabilities.

From the previously presented curves and results from literature [8], the following conclusions can be drawn:

There is an increasingly amount of stress-induced  $\varepsilon$  martensite being formed on regions 1 and 2. In region 3, due to martensite hardness and the increase in martensite volume during plastic deformation, strain hardening rate and coefficient increase even more since it starts deforming plastically. In region 4, the stress-induced martensitic transformation has already halted and the microstructure cannot maintain such a high strain hardening rate and coefficient, so it steadily falls until rupture.



**Figure 7.** X-ray diffraction pattern of stainless AISI 304 steel prior to deformation and with 0.1; 0.2; 0.3; 0.4 true strain values and after rupture.

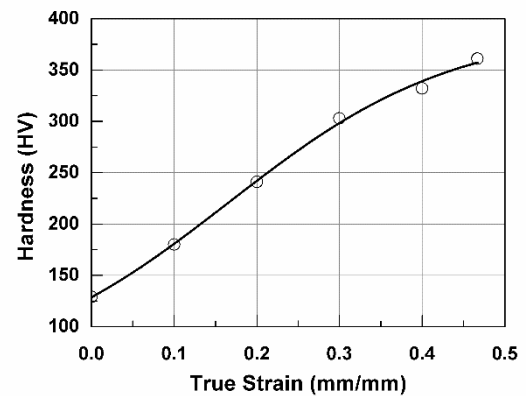


**Figure 8.** Hardness of stainless AISI 304 steel in function of true strain.

As discussed in earlier studies, the strain hardening behavior of AISI 304 steels depends strongly on the stress-induced martensitic transformation, which is heavily associated to austenite's stacking fault energy [8].

It is recommended that more investigation on this subject should be done, in order to complete this study and to understand the work hardening mechanisms. The presented method represents closely the real behavior of steel under a uniaxial load, and its results could certainly be considered for forming processes and numerical modelling [6].

## 4 CONCLUSION

In this work, the strain hardening behavior of dual phase, a non-grain oriented electrical and stainless AISI 304 steels was studied. Based on the results, the following conclusions can be drawn:

- (1) AISI 304 stainless steel exhibits higher tensile strength and ductility (TS = 800 MPa and  $\varepsilon_t = 67\%$ ) in comparison to the dual phase (TS = 664 MPa and  $\varepsilon_t = 34\%$ ) and non-grain oriented electrical steels (TS = 427 MPa and  $\varepsilon_t = 67\%$ ).
- (2) The instantaneous strain hardening coefficient of dual phase and non-grain oriented electrical steel increases at small strains, after the yield point, rapidly reaching its maximum and then steadily decreases until tensile strength.
- (3) Due to the stress-induced martensitic transformation, the instantaneous strain hardening coefficient of stainless AISI 304 keeps raising to high values and at large strains. Then, it rapidly decreases before reaching its tensile strength.
- (4) AISI 304 stainless steel shows higher instantaneous strain hardening coefficient values (between 0.2 and 0.8) and elongation (50%), what makes the strain hardening mechanism in this steel more efficient than the mechanisms in other two analysed steels.
- (5) More investigations are needed to clarify the strain hardening mechanisms of the steels analysed in this work. Microscopy techniques would certainly have success in characterize the microstructural evolution in response to deformation and lead to a better understanding of the strain hardening mechanisms. A Swift equation modified Crussard-Jaoul (C-J) analysis seems promising in this study.

## Acknowledgements

The authors thank the follow Brazilian agencies for the financial support: Coordenação de Aperfeiçoamento de Pessoal de Nível Superior (CAPES/PROEX), Conselho Nacional de Desenvolvimento Científico e Tecnológico (CNPq) and Pró-reitora de Pesquisa da Universidade Federal de Minas Gerais (PRPq UFMG).

## REFERENCES

- 1 Tahreen N, Zhang DF, Pan FS, Jiang XQ, Li C, Li DY, et al. Influence of yttrium content on phase formation and strain hardening behavior of Mg-Zn-Mn magnesium alloy. *Journal of Alloys and Compounds*. 2014. 615: 424-432
- 2 Ding H, Ding H, Song D, Tang Z, Yang P. Strain hardening behavior of a TRIP/TWIP steel with 18,8% Mn. *Materials Science and Engineering A*. 2011. 528: 868-873
- 3 Queiroz RRU. Envelhecimento Dinâmico em Aço Dual Phase de 600 MPa de Limite de Resistência. [ thesis ]. Belo Horizonte: Universidade Federal de Minas Gerais; 2013
- 4 Dieter GE. *Mechanical Metallurgy*. 3rd ed. London: McGraw-Hill Book Company; 1988
- 5 Cai M, Ding H, Tang Z, Lee H, Lee Y. Strain Hardening Behavior of High Performance FBDDP, TRIP and TWIP Steels. *Steel Research Int*. 2011. 3: 242-248
- 6 Paruz. H, Edmonds DV. The Strain Hardening Behaviour of Dual-phase Steel. *Materials Science and Engineering A*. 1989. 117: 67-74
- 7 *Standard Test Methods and Definitions for Mechanical Testing of Steel Products, A370 – 14*, ASTM International West Conshohocken; 2014
- 8 Gonzalez BM, Castro CSB, Bueno VTL, Vilela JMC, Andrade MS, Moraes JMD, et al. The influence of copper addition on the formability of AISI304 stainless steel. *Materials Science and Engineering A*. 2003. 343: 51-56
- 9 Jeong K, Jin J, Jung Y, Kang, Lee Y. *Acta Materialia*. 2013. 61: 3399-3410